

The effects of quadratic drag on the inverse cascade of two-dimensional turbulence

N. Gryanik, I. M. Held, K. S. Smith, and G. K. Vallis^{a)}
GFDL/Princeton University, Princeton, New Jersey 08542

(Received 3 September 2002; accepted 30 September 2003; published online 3 December 2003)

We explore the effects of a quadratic drag, similar to that used in bulk aerodynamic formulas, on the inverse cascade of homogeneous two-dimensional turbulence. If a two-dimensional fluid is forced at a relatively small scale, then an inverse cascade of energy will be generated that may then be arrested by such a drag at large scales. Both scaling arguments and numerical experiments support the idea that in a statistically steady state the length scale of energy-containing eddies will not then depend on the energy input to the system; rather, the only external parameter that defines this scale is the quadratic drag coefficient itself. A universal form of the spectrum is suggested, and numerical experiments are in good agreement. Further, the turbulent transfer of a passive tracer in the presence of a uniform gradient is well predicted by scaling arguments based solely on the energy cascade rate and the nonlinear drag coefficient. © 2004 American Institute of Physics.
 [DOI: 10.1063/1.1630054]

I. INTRODUCTION

The feature that most distinguishes two-dimensional turbulence from its three-dimensional counterpart is the presence of an inverse cascade of energy (see, e.g., Vallis¹ or Danilov and Gurarie² for reviews). Kraichnan³ was the first to predict that the inverse cascade should have a $k^{-5/3}$ energy spectrum, and there have since been a number of simulations that do show such a well-developed spectrum as well as, in some circumstances, some nonuniversal behavior (Frisch and Sulem,⁴ Maltrud and Vallis,⁵ Babiano *et al.*,⁶ Danilov and Gurarie,⁷ Boffetta *et al.*,⁸ and Smith *et al.*⁹). To obtain such a statistically steady universal spectrum in a finite domain there must be a frictional process that acts at large scales to halt the transfer of energy before the domain scale is reached as well as a good scale separation between the forcing scale and the frictional scale.

Normally (and especially in three-dimensional flows), frictional processes are considered to act at very small scales by way of molecular viscosity. Two-dimensional turbulence is a particular limit of quasigeostrophic turbulence that in turn arises in rapidly rotating, stratified flows. (There are some differences between quasigeostrophic flow, but at scales comparable to and larger than the deformation radius geostrophic turbulence theory suggests that the energy is transferred into the barotropic mode of the quasigeostrophic system, and this obeys the two-dimensional vorticity equation—see Salmon.¹⁰)

In such flows, Ekman layers generally exist at horizontal boundaries and, if the viscosity is uniform, their effects may be parametrized by a linear drag. Using such a drag in two-dimensional turbulence appears to be effective in arresting the inverse cascade in a smooth fashion, giving a well-

defined $-5/3$ inertial range between the forcing and frictional scales. (Sukoriansky *et al.*¹¹ document the possible pitfalls of using a less physical inverse hyperviscosity.) If the boundary layer is turbulent, then frictional effects are caused by vertical fluxes of horizontal momentum in three-dimensional turbulence. This has a much smaller spatial scale and much faster time scale than the nearly two-dimensional flow above the boundary layer, suggesting the use of a spatially varying eddy viscosity to parametrize the Reynolds stresses. This in turn leads to a quadratic drag to parametrize the bulk frictional effects of the boundary layer, rather than a linear drag, and, indeed, it is common practice to parametrize a well-mixed planetary boundary layer in this way (see, e.g., Holton¹² for more details). Note that the two-dimensional flow should then be considered the mean velocity, and the presence of the underlying surface defines the coordinate system in which the particular drag formulation is valid.

This form of drag is particularly interesting from a scaling-theory perspective, because the drag increases in strength as the intensity of the turbulence increases, and scaling arguments (given in Sec. III) suggest that the stopping scale is *independent* of the intensity of the forcing. In this paper our goal is to test this and other scaling predictions, and investigate whether the use of a quadratic drag is a robust and sensible notion in two-dimensional turbulence.

II. EQUATIONS OF MOTION

The momentum equation for constant density two-dimensional flow is

$$\frac{\partial \mathbf{u}}{\partial t} + \mathbf{u} \cdot \nabla \mathbf{u} = -\nabla p + \mathbf{F} - \mathbf{D}, \quad (1)$$

where \mathbf{u} is the velocity, p is the pressure, and \mathbf{F} and \mathbf{D} rep-

^{a)} Author to whom correspondence should be addressed. Electronic mail: gkv@princeton.edu

resent forcing and frictional terms and the density is taken to be one. Because the flow is incompressible, it is convenient to take the curl, giving the vorticity equation

$$\frac{\partial \zeta}{\partial t} + \mathbf{u} \cdot \nabla \zeta = F_\zeta + D_\zeta, \quad (2)$$

where $F_\zeta = \mathbf{k} \cdot \text{curl } \mathbf{F}$ and $D_\zeta = \mathbf{k} \cdot \text{curl } \mathbf{D}$. There are two parametrizations of the friction that we wish to focus on. One is the conventional linear drag, parametrizing an Ekman layer with constant diffusivity,

$$\mathbf{D} = -r\mathbf{u}, \quad (3)$$

so that

$$D_\zeta = -r\zeta, \quad (4)$$

where r has dimensions of inverse time. The second is the quadratic drag,

$$\mathbf{D} = -C_d |\mathbf{u}| \mathbf{u}, \quad (5)$$

so that

$$D_\zeta = -C_d \left(\frac{\partial |\mathbf{u}| v}{\partial x} - \frac{\partial |\mathbf{u}| u}{\partial y} \right), \quad (6)$$

where C_d has dimensions of inverse length. It is a combination of the usual nondimensional frictional parameter c_d and a boundary layer thickness h , $C_d = c_d/h$. As noted in the Introduction, this form of drag emerges in the parametrization of the turbulent atmospheric boundary layer. The mean flow, which we explicitly model, has large space and time scales and is strongly influenced by rotation so that its dynamics are approximately two dimensional. The fast component of the flow, on the other hand, has small spatial and time scales, is three dimensional, and it interacts with the slow component through the vertical fluxes of zonal momentum. The frictional effect of these fluxes can be parametrized by the bulk aerodynamic formula thus producing quadratic drag on the mean flow.

In rapidly rotating flow, such as the large-scale flow in the Earth's atmosphere or ocean, the stress need not be in a direction precisely opposite to that of the (geostrophic) wind, as is implied by (5); rather, it is at an angle because of the turning of the wind in the Ekman layer. However, this does not affect the scaling theory presented below. Also, in addition to these frictional terms, any numerical simulation of (2) at finite resolution must have a means of removing enstrophy at high wavenumbers, such as a conventional viscosity, a hyperviscosity, or a filter, but this is not the focus of this paper.

III. SCALING THEORY

A. Cascade phenomenology

Suppose that the forcing is isotropic and near monoscale—i.e., localized in (absolute) wavenumber space, near wavenumber k_f . Then we expect energy to cascade toward smaller wavenumbers, generating eddies of increasingly larger scale, while enstrophy cascades to the smaller scales. Nonlinear advective processes slow down as eddy size grows, so that at some wavenumber k_a (the “arrest”

wavenumber) energy removal due to friction becomes more efficient than energy transfer to the larger scales, and thus the inverse cascade is inhibited.

If $k_a \ll k \ll k_f$, then classical theory posits that the spectral energy flux ϵ is constant (through wavenumber space) and that spectral energy depends only on the rate at which energy is cascaded, ϵ , and local isotropic wavenumber, leading to the well-known spectrum

$$E(k) = C \epsilon^{2/3} k^{-5/3}. \quad (7)$$

Here C is the Kolmogorov–Kraichnan constant, which experimentally has been found to lie in the range 4–6 (Maltrud and Vallis,⁵ Chekhlov *et al.*,¹³ Danilov and Gurarie,² and Smith *et al.*⁹). The associated inertial time scale is given by

$$T_{\text{adv}} \sim [kV(k)]^{-1} \sim k^{-2/3} \epsilon^{-1/3}, \quad (8)$$

where $V(k)$ is the velocity at wavenumber k . The frictional timescale, based on the same energy spectrum, is

$$T_{\text{drag}}(k) \sim [C_d V(k)]^{-1} \sim C_d^{-1} k^{1/3} \epsilon^{-1/3}, \quad (9)$$

for quadratic drag and

$$T_{\text{drag}}(k) \sim r^{-1}, \quad (10)$$

for linear drag. There is a qualitative difference between these two timescales in that the scaling with quadratic drag is scale selective while with linear drag it is not. The inverse cascade stops at the scale where dissipative processes become as fast as nonlinear advection. This gives us scalings for arrest wavenumbers,

$$k_a = A_l \left(\frac{r^3}{\epsilon} \right)^{1/2}, \quad (11)$$

for linear drag, and

$$k_a = A_n C_d, \quad (12)$$

for quadratic drag, where A_l and A_n are nondimensional coefficients. In the quadratic drag case the arrest wavenumber is *independent* of the strength of forcing ϵ and depends, linearly, on the drag coefficient alone.

Relationship (11) has been found to be a satisfactory approximation by Smith *et al.*,⁹ although with a large value of the nondimensional coefficient A_l . Using two slightly different assumptions about the form of the energy spectrum near the stopping scale, Smith *et al.*⁹ offer two predictions for A_l , namely $A_l = (3C)^{3/2} \approx 76$ and $A_l = (9C/5)^{3/2} \approx 35$ (using $C = 6$), with slightly better numerical agreement with the lower value. Using these, we can make a rough prediction for A_n , as follows. The nonlinear drag has the approximate form

$$D_\zeta = -C_d |v| \zeta, \quad (13)$$

where $|v|$ is the rms velocity of the flow, and indeed a few test simulations using (13) gave the same scaling behavior as those with the full drag, (6). Thus, for any given simulation, the nonlinear drag behaves as if it were a linear drag with value $r_{\text{eff}} = C_d |v|$. If $|v|$ is taken to be the velocity at the arrest scale itself, then

$$r_{\text{eff}} = C_d |v| \approx C_d (3C/2)^{1/2} (\epsilon/k_a)^{1/3}, \quad (14)$$

and using this in (11) gives

$$k_a \approx C_d [A_l^{2/3} (3C/2)^{1/2}] = C_d [(3/2)^{1/2} \alpha C^{3/2}]. \quad (15)$$

where $\alpha=3$ or $9/5$, being the two values used for A_l . This gives values of $A_n=32.4$ (corresponding to $\alpha=9/5$) or $A_n=54$ (corresponding to $\alpha=3$), taking $C=6$. Although the approximations inherent in this calculation (including that of the value of A_l) militate against its quantitative accuracy, they do indicate that a value of A_n much greater than unity is to be expected.

Held¹⁴ discussed scalings analogous to (12) in order to estimate possible stopping scales for the inverse cascade in the atmosphere. In the atmospheric boundary layer, $c_d \sim 10^{-3}$ over the ocean surface and $h \sim 1-2$ km, so that $C_d \sim 10^{-6} \text{ m}^{-1}$. One might roughly estimate a stopping scale to be of order a few thousand kilometers. However, the presence of nondimensional coefficients, the difference between the geostrophic wind and the near-surface wind, and the presence of potential energy in the atmosphere will all act to make such estimates quantitatively unreliable.

B. Turbulent diffusivity

Let us now consider the problem of the turbulent diffusivity of the flows described above. Specifically, we consider the transport of a passive tracer, with a mean gradient, stirred by the homogeneous turbulent flow. Thus, the tracer variance is maintained against high-wavenumber dissipation by a uniform meridional gradient, while the tracer itself is stirred by the eddies. The evolution of the tracer fluctuation, ϕ , is then described by the equation

$$\frac{\partial \phi}{\partial t} + J(\psi, \phi) + \gamma v = D \phi, \quad (16)$$

where $\gamma = \partial \bar{\phi} / \partial y$ is the fixed mean tracer gradient. Note that (16) follows when we apply the tracer transport equation to the full tracer field that consists of the mean component γy and the fluctuation ϕ . The total amount of tracer quantity is fixed, and in statistical equilibrium the tracer variance is maintained by a balance between dissipation $D \phi$ and the tracer variance created through the presence of a mean gradient, so that

$$\frac{d \overline{\phi^2/2}}{dt} = \overline{\gamma v \phi} - \overline{D \phi^2} = 0. \quad (17)$$

The tracer variance production $\overline{\gamma v \phi}$ occurs primarily at the energy-containing scale because the velocity spectrum is peaked there. When the equilibrium state is well established for both velocity and tracer fields, then at scales within the energy inertial range dimensional analysis suggests that the spectrum of tracer variance should have a $-5/3$ slope.

The meridional transport of the tracer may be parametrized by the formula

$$\overline{v \phi} = \gamma D, \quad (18)$$

which may be taken as a *definition* of the eddy diffusivity D . Because the flow is homogeneous, D is a constant. If such a formula is to have any predictive use, we need to be able to estimate D from the properties of the turbulent flow. Since D has dimensions $[UL]$, we expect that, if the energy spectrum

is sufficiently sharply peaked, L should be the energy-containing scale, namely $L \sim k_a^{-1}$, and U the magnitude of the velocity at that scale, namely $U = [E(k_a)k_a]^{1/2}$, where k_a is the arrest scale. We then arrive at a scaling for the eddy diffusivity in the case when quadratic drag arrests the inverse cascade,

$$D \sim \epsilon^{1/3} k_a^{-4/3} \sim \epsilon^{1/3} C_d^{-4/3}. \quad (19)$$

Alternatively, we may simply posit that the tracer transport in such a case is determined solely by the two parameters in the problem, namely ϵ and C_d . Dimensional analysis then immediately leads to (19), noting that the tracer gradient γ may, without loss of generality, be eliminated from the problem by a simple rescaling of ϕ , because (16) is linear in ϕ .

IV. NUMERICAL EXPERIMENTS

A. Energy spectra and arrest scale

Numerical simulations were performed using a dealiased two-dimensional spectral model, integrating (2) in a doubly periodic domain with maximum wavenumber 255 and approximate equivalent gridpoint resolution 512^2 . The forcing was a random Markovian forcing localized at the isotropic wavenumber $k_f=160$, as in Maltrud and Vallis.⁵ Coherent structures are not explicitly suppressed by such a forcing, and typically may occur at scales comparable to the forcing itself—see Oetzel.¹⁵ Large-scale coherent vortices do not form Fig. 4. In order to dissipate the enstrophy that cascades to the small scales, an exponential cutoff filter was applied, with cutoff wavenumber $k_{\text{cut}}=200$, following Smith *et al.*⁹

The first set of experiments that we present here explores how the arrest scale depends on the drag coefficient and the energy injection rate. For this purpose we fix the quadratic drag coefficient at a nondimensional value of $\tilde{C}_d = C_d k_f^{-1} = 3.75 \times 10^{-3}$, with an overtilde ($\tilde{}$) denoting the nondimensional value, while the energy generation rate is varied by a factor of 100, so that any changes in the shape of the kinetic energy spectrum can be attributed to the change in energy flux. Figure 1 shows steady-state energy spectra for three runs R1, R2, R3 forced at the wavenumber $k_f=160$, with an energy generation rate (measured in units of $L^2 T^{-3}$) equal to $g=0.1, 1, 10$, respectively. (The energy generation rate differs slightly from the inverse cascade rate because some of the energy input is lost to small-scale dissipation.) In the inertial range $k_a < k < k_f$ all three spectra show good agreement with Kolmogorov's energy spectrum $C \epsilon^{2/3} k^{-5/3}$; the best fit found for Kolmogorov's constant is about 5. As expected, the spectra all seem to peak at the same wavenumber $k_a=31$. To see this most clearly, we rescale every energy spectrum by the appropriate value of $\epsilon^{-2/3}$. The predicted value of this energy spectrum is then simply $E_{\text{new}}(k) = \epsilon^{-2/3} E(k) = C k^{-5/3}$. The rescaled spectra do fall on top of each other as shown in Fig. 1(b), even for scales at or larger than the arrest scale, where friction is expected to be important. To contrast this behavior with the high sensitivity to the change in the energy forcing exhibited by linear drag, we conducted similar experiments with linear friction. Now linear drag was fixed at $r=0.2$ (again to produce a sensible

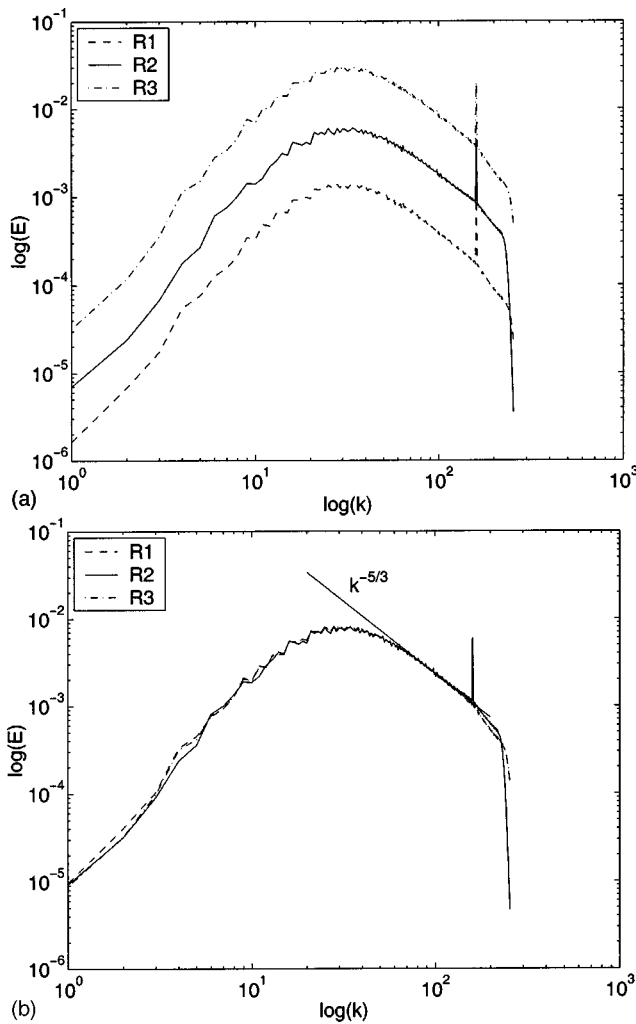


FIG. 1. (a) Steady-state kinetic energy spectra obtained by variation of forcing parameter ϵ (energy flux) while the quadratic drag coefficient is fixed at $C_d=0.6$; $\epsilon=0.1, 1, 10$ for experiments R1, R2, R3. Note that the stopping scale is independent of the energy flux. (b) The same spectra, but now rescaled by an appropriate value of the energy flux, ϵ : $E_{\text{new}}(k) = \epsilon^{-2/3} E(k)$.

stopping scale) and the energy generation rate assumed values $g=0.5, 1, 2$ for runs L1, L2, L3 shown in Fig. 2. The rescaled energy spectra in Fig. 2(b) clearly demonstrate that rescaled spectra coincide only in the energy inertial range, and that the energy peaks are well separated and the arrest wavenumber gets smaller as the generation rate increases, in agreement with (11).

The scaling analysis of Sec. III suggests that the arrest scale of the inverse cascade should depend inversely on the quadratic drag coefficient [see (12)]. We tested this using a sequence of experiments in which the energy input rate was held at a unit value, and the drag was varied, with values of \tilde{C}_d in the range $(0.625-12.5) \times 10^{-3}$. The arrest wavenumber is determined as the wavenumber where the energy spectrum peaks. Figure 3 shows the experimental and predicted arrest wavenumber as a function of the drag coefficients. A very good linear fit is apparent, in accord with the theory, with an empirical scaling factor of about 51—that is, $k_a \approx 51C_d$. Evidently, just as in the case with a linear drag,

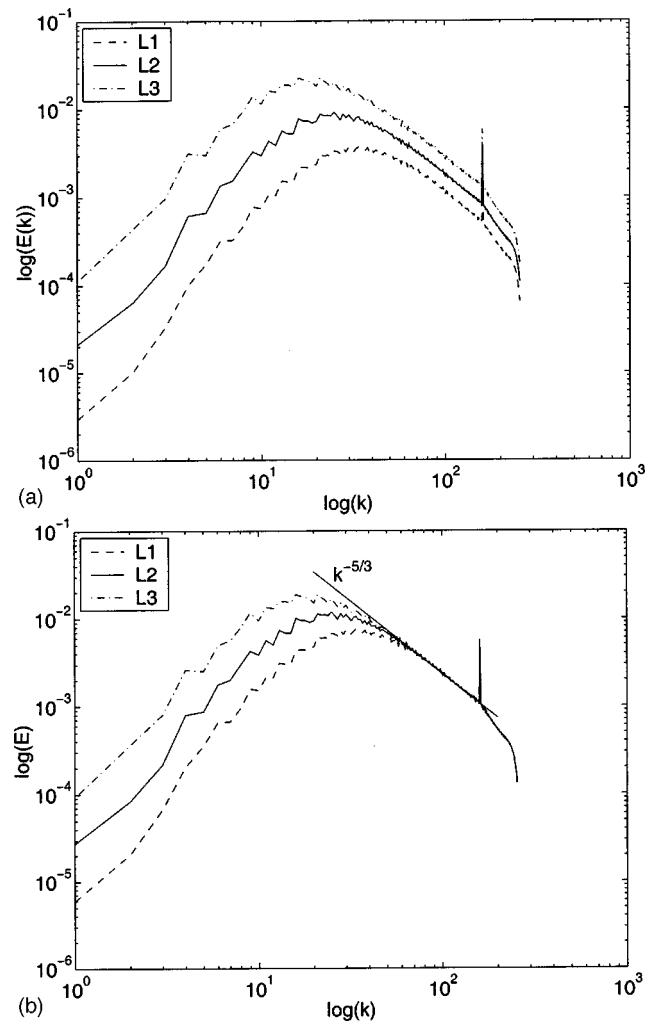


FIG. 2. Same as Fig. 1 but using linear drag to halt the inverse cascade. (a) Energy spectra with linear drag coefficient $r=0.2$ and energy forcing of $\epsilon=0.5, 1, 2$ for runs L1, L2, L3. Note that the stopping scale moves to larger scales as the energy flux increases. (b) Rescaled spectra, $E_{\text{new}}(k) = \epsilon^{-2/3} E(k)$.

Smith *et al.*,⁹ and as predicted in Sec. III, a large nondimensional coefficient, relates the two scales. As the value of quadratic drag increases the stopping scale moves closer to the forcing scale and the underlying assumption of our analysis that these scales are well separated fails. In this case we cannot expect the prediction to work, and it is clear from the plot that the prediction does not hold for stopping wavenumbers larger than $0.4k_f$.

In common with previous simulations of the inverse cascade [see, for example, Fig. 1(e) of Maltrud and Vallis⁵], the vorticity field in our experiments does not show much large-scale structure (Fig. 4). In particular, we do not observe the formation of strong local vorticity maxima at all scales reported by Borue¹⁶ in his experiments with an inverse hyperviscosity acting as a large-scale dissipation. Borue¹⁶ connects the existence of these vortex structures with significant deviation of his energy spectrum from the universal $k^{-5/3}$ form. In some test cases we extended our integration to 2000 eddy turnover times, several times longer than is needed for statistical equilibration, and we found that no pronounced modi-

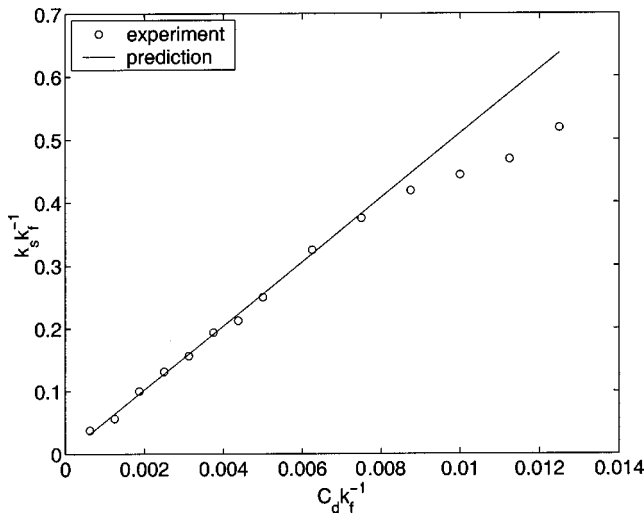


FIG. 3. The arrest scale, i.e., the spectral energy peak of the inverse cascade, as a function of the quadratic drag coefficient C_d . The circles are experimental values, the solid line is the scaling prediction using (12).

fication in the energy spectrum occurs after equilibration was achieved. Figure 5(a) illustrates this point: it shows the energy spectrum averaged over the time period following the equilibration (solid line) and the maximum and minimum deviations from the average that occur in this time period, neither of which occur at either end of that period. That is to say, there is no trend in the energy spectrum, and we conclude that our simulations are well equilibrated.

B. Calculation of diffusivity

In all cases of the numerical integration of the model with a tracer [i.e., (2) and (16)], the meridional tracer gradient, γ , is set to unity. The small-scale dissipation of the tracer

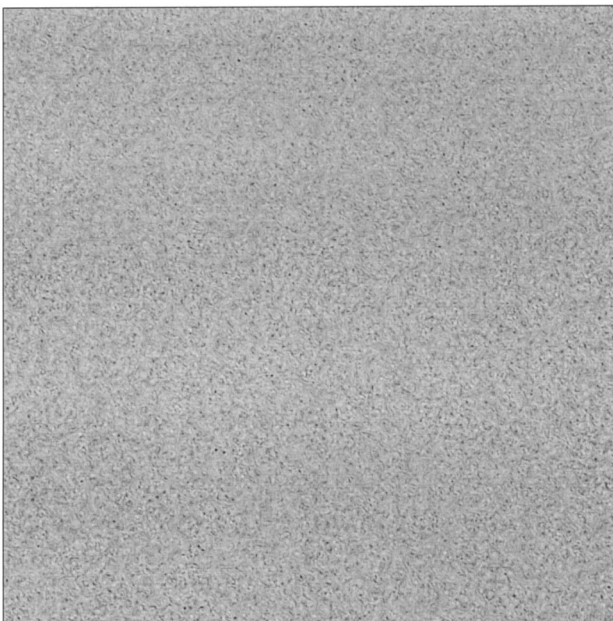


FIG. 4. A snapshot of the vorticity field in physical space in a typical integration. The value of vorticity varies in the range $|\zeta/(\epsilon^{1/3} k_f^{2/3})| \leq 19.2$.

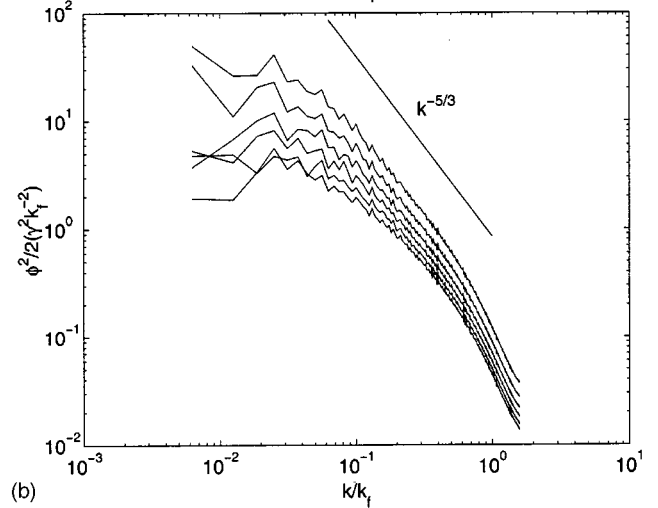
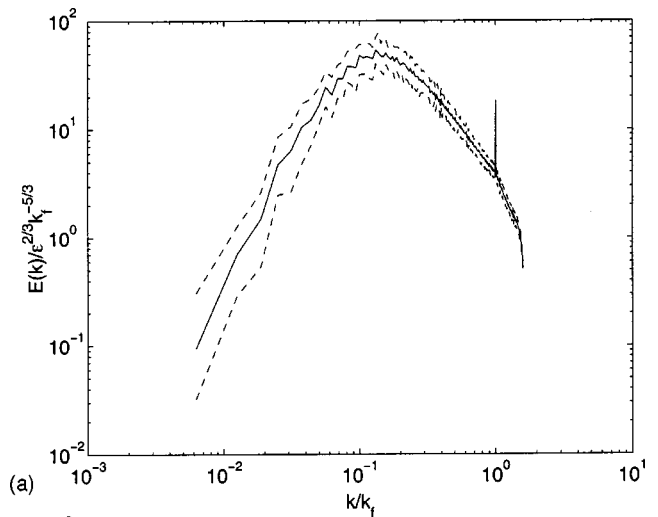


FIG. 5. (a) Time-averaged energy spectrum in the extended run (solid) and maximum deviations from it (dashed). (b) Time-averaged tracer variance spectra with various values of energy input ϵ .

is accomplished by the cutoff filter of the same form as that used for the enstrophy removal at the small scales. Test cases indicate that the precise choice of filter (or use of hyperviscosity) has little effect on the large-scale eddy transport properties.

The nondimensionalized tracer variance spectra,

$$\overline{\phi^2/2} = \gamma^{-2} k_f^2 \overline{\phi^2/2}, \tag{20}$$

are plotted in Fig. 5(b). The amplitude of the tracer variance decreases with decreasing energy levels or increasing drag coefficients. All of the tracer spectra peak at the wavenumber that is smaller than the stopping wavenumber. Figure 6 shows diffusivities D that are calculated directly from the model tracer and velocity fields, plotted as a function of the predicted value. The diffusivity and predicted value are nondimensionalized according to $\tilde{D} = \epsilon_0^{-1/3} k_f^{4/3} D$ and $\epsilon^{1/3} \tilde{C}_d^{-4/3} = \epsilon^{1/3} C_d^{-4/3} / (\epsilon_0^{1/3} k_f^{-4/3})$, where ϵ_0 is the energy input in a control experiment. As is clear from the graph, a good linear relationship is obtained between the predicted value and the experiment. As we might expect the deviations between the experimental

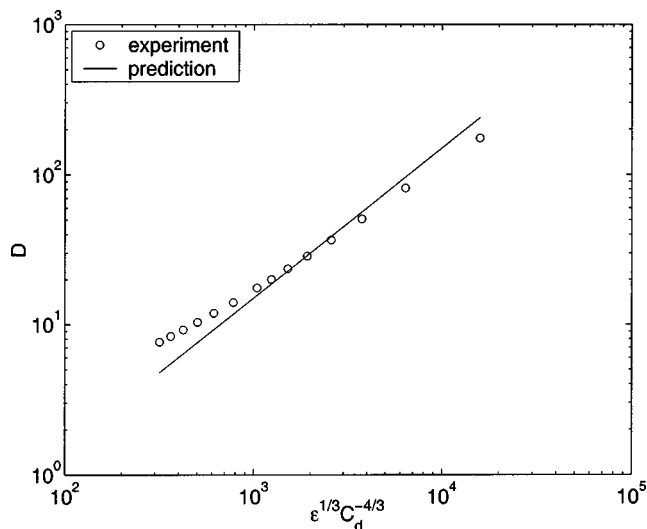


FIG. 6. Value of eddy diffusivity D plotted against its predicted value $\epsilon^{1/3} C_d^{-4/3}$ (both values are divided by $\epsilon_0^{1/3} k_f^{-4/3}$ to make them nondimensional). The circles are the experimental values and the solid line is the prediction.

and predicted values grows as the scale separation between the arrest wavenumber and forcing wavenumber decreases.

V. CONCLUSIONS

A quadratic drag parametrization of the effect of the boundary layer stresses on a two-dimensional fluid was employed to arrest the inverse energy cascade of the two-dimensional turbulent flows. Phenomenological scaling theory suggests that the arrest scale of the inverse cascade, and so the energy-containing scale of the turbulence, will vary inversely with the quadratic drag coefficient and be independent of the magnitude of the energy input. Numerical experiments confirm this prediction over a fairly broad parameter range.

We further predict an eddy diffusivity based on the scale of the energy-containing eddies and the velocity magnitude at that scale, giving a transport that depends solely on the drag coefficient and the rate of energy input. The resulting scaling for the eddy transport shows good skill in the case in which a turbulent velocity field stirs a tracer superimposed on a uniform meridional tracer gradient. In this case there is a well-defined energy scale and a good scale separation between the scale of the eddies and the characteristic scale of the mean gradient of the tracer field (because the mean gradient is linear, this scale separation is, in fact, infinite). These two features together likely account for the good performance of the diffusive theory.

The main conclusions of our study are thus the following: (i) we confirm the relatively robust nature of the inverse cascade of two-dimensional turbulence, given a good scale separation between forcing scales, energy-containing scales, and domain scales, as well as the relative lack of obvious large-scale coherent structures in such a flow; (ii) we find that a quadratic drag is a physically reasonable way to halt the inverse cascade, giving rise to an arrest scale, and thus an energy-containing scale, that depends solely on the drag coefficient itself, and so that is independent of the rate of energy input; (iii) we find that the transport of a passive tracer in such a flow is well predicted using phenomenological scaling arguments, again provided there is a good separation between the forcing scale, energy-containing scale, and tracer gradient scale.

- ¹G. K. Vallis, "Problems and phenomenology in two-dimensional turbulence," *Nonlinear Phenomena in Atmospheric and Oceanic Sciences*, edited by C. F. Carnevale and R. Pierrehumbert (Springer-Verlag, Berlin, 1993), pp. 1–25.
- ²S. Danilov and D. Gurarie, "Quasi-two-dimensional turbulence," *Usp. Fiz. Nauk* **170**, 921 (2000).
- ³R. H. Kraichnan, "Inertial ranges in two-dimensional turbulence," *Phys. Fluids* **10**, 1417 (1967).
- ⁴U. Frisch and P. L. Sulem, "Numerical simulation of the inverse cascade in two-dimensional turbulence," *Phys. Fluids* **27**, 1921 (1984).
- ⁵M. E. Maltrud and G. K. Vallis, "Energy spectra and coherent structures in forced two-dimensional and beta-plane turbulence," *J. Fluid Mech.* **228**, 321 (1991).
- ⁶A. Babiano, B. Dubrulle, and P. Frick, "Some properties of two-dimensional inverse energy cascade dynamics," *Phys. Rev. E* **55**, 2693 (1997).
- ⁷S. Danilov and D. Gurarie, "Nonuniversal features of forced two-dimensional turbulence in the energy range," *Phys. Rev. E* **63**, 020203 (2001).
- ⁸G. Boffetta, A. Celani, and M. Vergassola, "Inverse energy cascade in two-dimensional turbulence: Deviations from Gaussian behavior," *Phys. Rev. E* **61**, 29 (2000).
- ⁹K. S. Smith, G. Boccaletti, C. C. Henning, I. N. Marinov, C. Y. Tam, I. M. Held, and G. K. Vallis, "Turbulent diffusion in the geostrophic inverse cascade," *J. Fluid Mech.* **469**, 13 (2002).
- ¹⁰R. S. Salmon, *Lectures on Geophysical Fluid Dynamics* (Oxford University Press, New York, 1998), p. 378.
- ¹¹S. Sukoriansky, B. Galperin, and A. Chekhlov, "Large scale drag representation in simulations of two-dimensional turbulence," *Phys. Fluids* **11**, 3043 (1999).
- ¹²J. R. Holton, *An Introduction to Dynamic Meteorology*, 3rd ed. (Academic, San Diego, 1992), pp. 124–126.
- ¹³A. Chekhlov, S. A. Orszag, S. Sukoriansky, B. Galperin, and I. Staroselsky, "Direct numerical simulation tests of eddy viscosity in two dimensions," *Phys. Fluids* **6**, 2548 (1994).
- ¹⁴I. M. Held, "The macroturbulence of the atmosphere," *Tellus* **51A-B**, 59 (1999).
- ¹⁵K. Oetzel and G. K. Vallis, "Strain, vortices, and the enstrophy inertial range in two-dimensional turbulence," *Phys. Fluids* **9**, 2991 (1997).
- ¹⁶V. Borue, "Inverse energy cascade in stationary two-dimensional homogeneous turbulence," *Phys. Rev. Lett.* **72**, 1475 (1994).